Chapter 11
LEAP-ASIA-2019 Centrifuge Test at NCU

Jun-Xue Huang and Wen-Yi Hung

Abstract Two centrifuge tests are performed at NCU under centrifugal acceleration field of 26*g* and 13*g* to validate the generalized scaling law for LEAP-ASIA-2019. The model arrangement and test process follow the specification of LEAP-UCD-2017. Both models are subjected one destructive motion which is 0.18*g*, 1 Hz, 16 cycles, tapered sine wave. Test results indicate the model adopted generalized scaling law with virtual 1*g* modeling factor of 2 can generally simulated the same prototype of the model only adopted centrifuge scaling law. The acceleration response, pore water pressure behavior, and cone tip resistance of both models are in good agreement with each other.

Keywords Liquefaction Experiments and Analysis Project (LEAP-ASIA-2019) · Generalized scaling law (GSL) · Centrifuge modelling

11.1 Introduction

Liquefaction Experiments and Analysis Projects (LEAP) is a series of collaborative research projects, and LEAP aims to produce reliable experimental data for assessment, calibration, and validation of constitutive models and numerical modeling techniques (Kutter et al., 2020a). In LEAP-UCD-2017, 9 different centrifuge facilities conducted 24 separate model tests to obtain the meaningful assessment of the sensitivity and variability of the tests (Kutter et al., 2020b).

For LEAP-ASIA-2019, NCU conducted two centrifuge modeling tests to validate the generalized scaling law. The acceleration response, excess pore water pressure behavior, displacement behavior, and cone tip resistance of model A and model B are compared and discussed in this paper. In addition, the shear velocity and predominate frequency of soil deposit determined by pre-shaking technique and the deposit profile movement tracked by spaghettis are presented.

J.-X. Huang (✉) · W.-Y. Hung
Department of Civil Engineering, National Central University, Taoyuan, Taiwan

T. Tobita et al. (eds.), *Model Tests and Numerical Simulations of Liquefaction and Lateral Spreading II*, https://doi.org/10.1007/978-3-031-48821-4_11

11.2 Test Equipment and Material

NCU geotechnical centrifuge has nominal radius of 3 m. The one-dimensional shaker was equipped on the basket of centrifuge. The maximum payload of shaker is 400 kg under maximum centrifugal acceleration field of 80*g*. The shaker can provide a motion with frequency range from 0 to 250 Hz. The container used for LEAP-ASIA-2019 is a rigid box composed by aluminum alloy plates with inner dimensions of 767 mm (L) × 355 mm (W) × 400 (H). The detail information could refer to Hung et al. (2022).

Ottawa sand F65 shipped from UC Davis is used to make the dry sand bed for LEAP-ASIA-2019. The value recommended by Carey et al. (2020) of minimum dry density and maximum dry density is 1490.5 kg/m^3 and 1757.0 kg/m^3, respectively. Ottawa sand F65 is classified as poorly graded sand in Unified Soil Classification System. The detail information regarding to the physical and mechanical properties of Ottawa sand F65 were presented by Carey et al. (2020) and El Ghoraiby et al. (2020).

11.3 Description of the Experiments

Two tests for LEAP-ASIA-2019 were conducted at National Central University (NCU) and the testing conditions are listed at Table 11.1. The dimensions of model are 767 mm (L) × 355 mm (W) × 153.8 mm (H) with 1643 kg/m^3 (model A) and 1626 kg/m^3 (model B) of dry unit weight by using Ottawa F-65 sand. A 5-degree slope and curvature ground surface are the same as the models of LEAP-UCD-2017. The centrifuge modeling factor, η, are 26 and 13; and the virtual 1*g* modeling scaling factor, μ, are 1 and 2 for model A and B, respectively. Therefore, models A and B were carried out under 26*g* and 13*g* acceleration field. Based on the generalized scaling law provided by Iai et al. (2005), the scaling factors of physical quantities adopted in NCU tests are listed in Table 11.2.

During spinning, total 3 shaking events were applied including 1 destructive and 2 nondestructive motions. The destructive 16-cycle tapered sine wave was 1 Hz frequency and target effective peak base acceleration (PBA_{eff}) of about 0.1*g*. Before and after destructive motion, two nondestructive motions with 3 Hz frequency and 0.04*g* amplitude of 1-cycle sine wave were input to detect the shear velocity and predominant frequency of soil strata. The characteristics of shaking events are listed

Table 11.1 Conditions of models

Test no.	Scaling factor		Achieved density (kg/m^3)	PBA (g)	PBA_{eff} (g)	PBA_{1Hz} (g)
	Centrifuge, η	Virtual 1*g*, μ				
Model A	26	1	1643	0.180	0.141	0.108
Model B	13	2	1628	0.164	0.126	0.096

Table 11.2 Scaling factors adopted for NCU models

Physical quantity	Generalized scaling factor	Model A	Model B
Length	$\mu\eta$	26	26
Density	1	1	1
Time	$\mu^{0.75}\eta$	26	21.8
Frequency	$\mu^{-0.75}/\eta$	1/26	1/21.8
Acceleration	$1/\eta$	1/26	1/13
Velocity	$\mu^{0.75}$	1	1.68
Displacement	$\mu^{1.5}\eta$	26	36.8
Stress	μ	1	2
Strain	$\mu^{0.5}$	1	1.41
Stiffness	$\mu^{0.5}$	1	1.41
Permeability	$\mu^{0.75}\eta$	26	21.8
Pore pressure	μ	1	2

Table 11.3 Characteristics of three shaking events

Event no.	Frequency (Hz)	PBA (model A / model B)	Cycle	Type
s1	3	0.036*g*/0.045*g*	1	Pre-shaking (nondestructive) Rectangular sine wave
s2	1	0.180*g*/0.164*g*	16	Main shaking (destructive) Tapered sine wave
s3	3	0.035*g*/0.046*g*	1	Pre-shaking (nondestructive) Rectangular sine wave

in Table 11.3. The achieved PBA_{eff} of destructive motions are 0.141*g* and 0.126*g* for models A and B, respectively.

The models were prepared and following the test procedure of LEAP-UCD-2017, the test flow chart is shown in Fig. 11.1 (Kutter et al., 2020a). The sand bed was made by air-pluviation method with a constant drop height of 500 mm and flow rate of 2.5 kg/min. The accelerometers and pore pressure transducers were installed at a specific location during pluviating. The 5° slope and curved surface were formed by using a vacuum and a specific curved acrylic scraper after air-pluviation completed. Eighteen PVC surface markers were then placed and 12 sticks of spaghetti were penetrated vertically into soil strata at the certain locations. The side view and top view of model A and model B before test are shown in Figs. 11.2 and 11.3, respectively.

Pure CO_2 was filled from the bottom of the container for 1.5 h with air flow rate of 0.25 kg/cm^2 to replace the air in the container before saturation. The methylcellulose solution with specific viscosity was dropped on the sponge putting on the slope surface to saturate model with a flow rate of 1 kg/h under stable vacuum pressure. The degree of saturation was measured by Okamura method and it should be higher than 99.5%. Then the location and elevation of markers were measured by using digital vernier caliper.

NCU centrifuge was spinning from 1*g* to certain g-level (26*g* for model A and 13*g* for model B), and the tests were carried out by the sequence described below;

Fig. 11.1 The procedure of LEAP tests at National Central University. (**a**) Top view of dry model; (**b**) Curved surface; (**c**) Side view of dry model; (**d**) Side view of saturated model; (**e**) Top view of saturated model

(1) the first shaking event, a nondestructive motion, was inputted; (2) the first CPT test was implemented; (3) second shaking event, a destructive motion, was input; (4) the second CPT test was implemented; (5) the third shaking event, a nondestructive motion, was input. After testing, the centrifuge was stopped to measure the final location and elevation of makers and cut the soil profile to observe deformation behavior of spaghetti and the position of pore pressure transducers at the middle array. The soil profiles of model A and model B after test are shown in Figs. 11.4 and 11.5, respectively. In addition, the detail information regarding to air-pluviation, saturation, and in-flight cone penetration test were presented by Hung and Liao (2020).

Finally, the achieved PBA_{eff} of destructive motions are 0.112 and 0.104*g* in model A and B, respectively.

11.4 Comparison Between Model A and Model B

The positions of sensors and the direction of positive acceleration are shown in Fig. 11.6. The positive acceleration is toward upslope direction, conversely, the negative acceleration is toward downslope direction. This is the definition of the

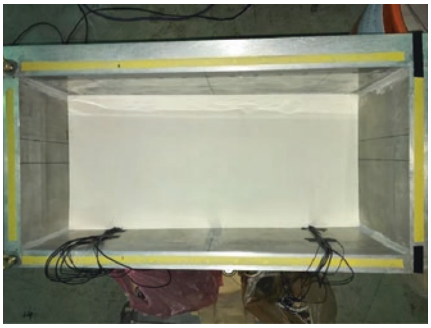

(a) Top view of dry model

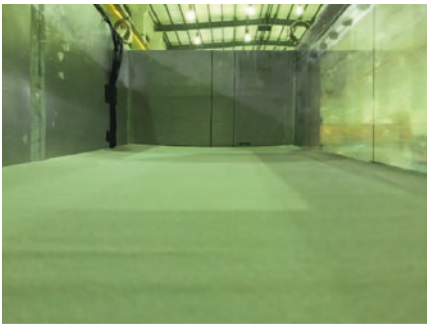

(b) Curved surface

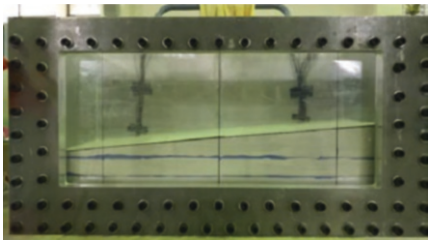

(c) Side view of dry model

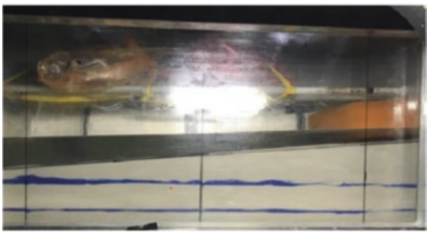

(d) Side view of saturated model

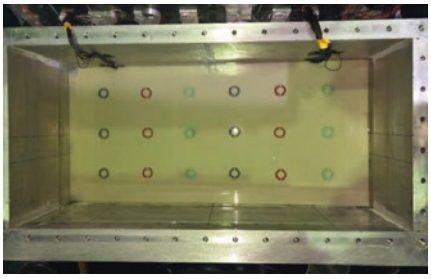

(e) Top view of saturated model

Fig. 11.2 Model A photos before test. (**a**) Side view; (**b**) Side view before profile cutting; (**c**) Profile cutting for spaghettis; (**d**) Profile cutting for middle array pore pressure transducers

direction of results in this paper, and all of the results in this paper are presented in prototype scale.

11.4.1 Acceleration Response

Figure 11.7 is the acceleration time histories of destructive motion 1 in model A and model B. The acceleration is expressed in prototype scale by taking scaling factor of 1/26 ($\eta = 26$) in model A and 1/13 ($\eta = 13$) in model B. The time histories indicate that the acceleration response of both models is very consistent; however, there is a slightly different of spike signal amplitude obtained by the accelerometers at the surface layer.

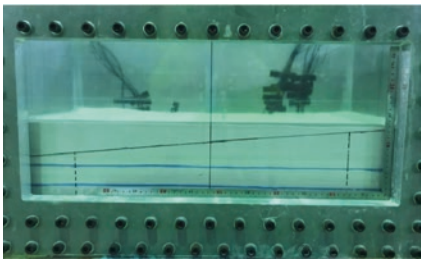

(a) Side view of dry model

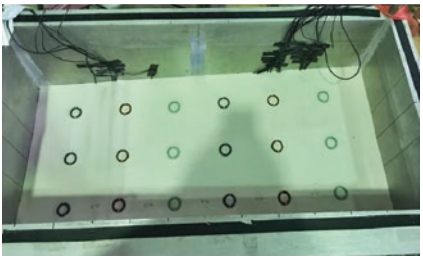

(b) Top view of dry model

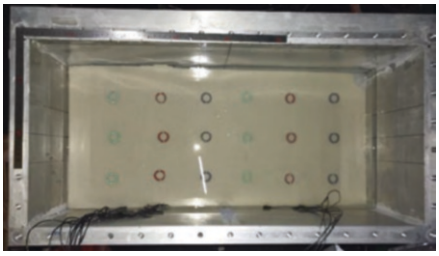

(c) Top view of saturated model

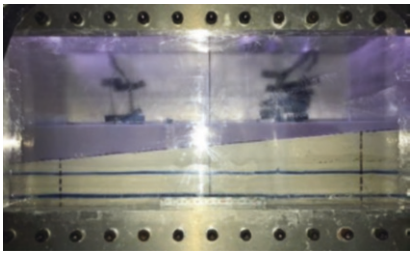

(d) Side view of saturated model

Fig. 11.3 Model B profile before test. (**a**) Side view before profile cutting; (**b**) Profile cutting for spaghetti; (**c**) Profile cutting for middle array pore pressure transducers

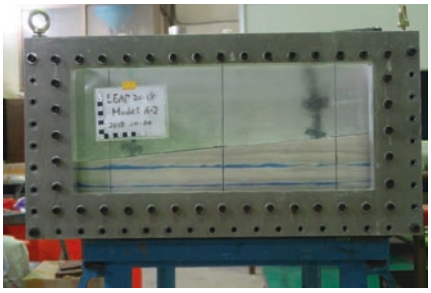

(a) Side view

(b) Side view before profile cutting

(c) Profile cutting for spaghettis

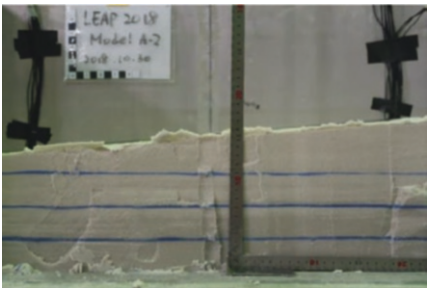

(d) Profile cutting for middle array pore pressure transducers

Fig. 11.4 Model A photos after test. (**a**) Side view of dry model; (**b**) Top view of dry model; (**c**) Top view of saturated model; (**d**) Side view of saturated model

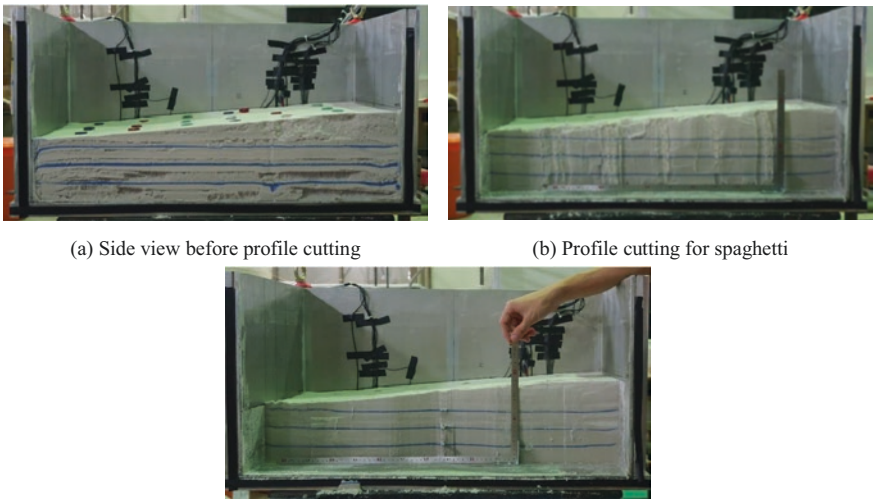

(a) Side view before profile cutting

(b) Profile cutting for spaghetti

(c) Profile cutting for middle array pore pressure transducers

Fig. 11.5 Model B photos after test

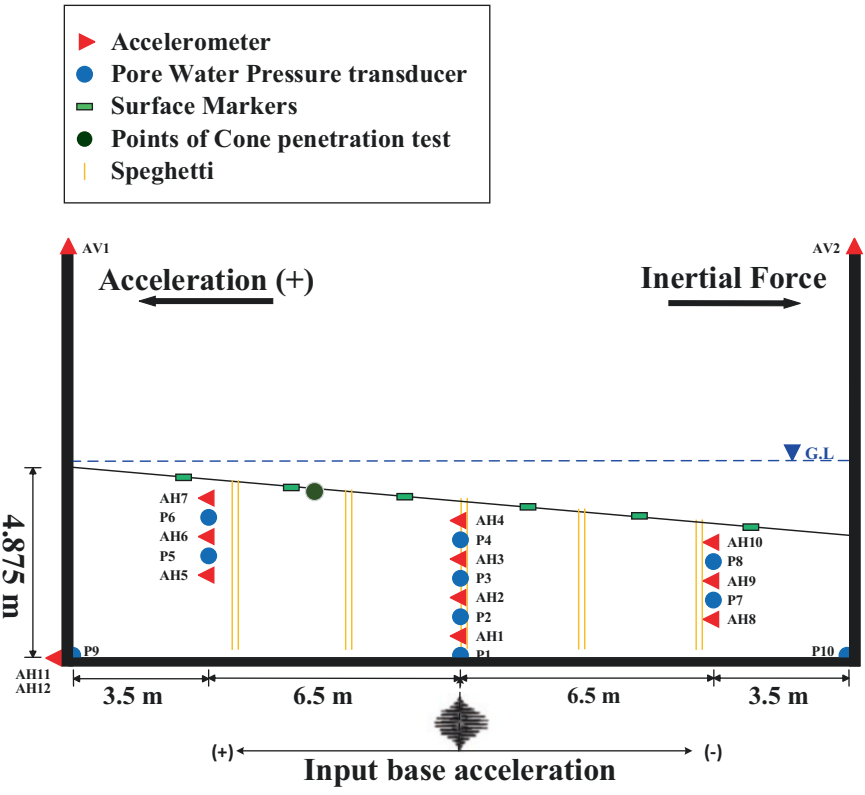

Fig. 11.6 Model arrangement and direction definition of NCU models

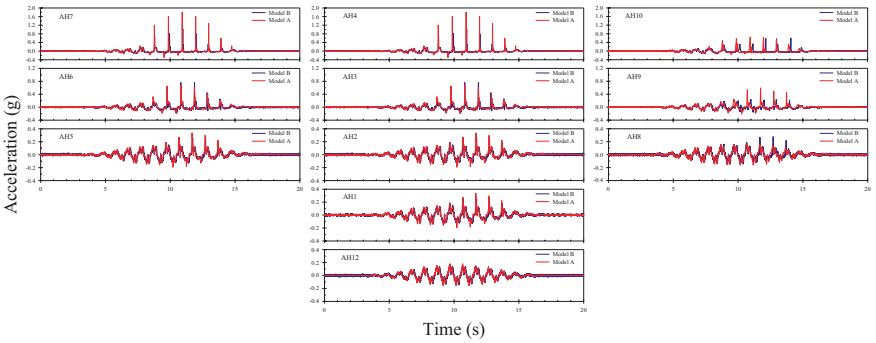

Fig. 11.7 Acceleration time histories of main shaking (s2)

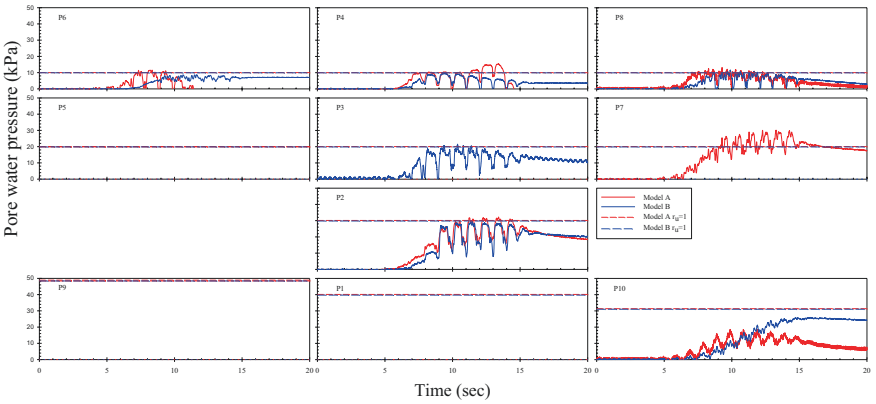

Fig. 11.8 Excess pore water pressure time histories (20 s) of main shaking (s2)

11.4.2 EPWP Behavior

Figure 11.8 shows the excess pore water pressure exceeding behavior during destructive motion 1 in model A and model B. The EPWP is expressed in prototype scale by taking scaling factor of 1 ($\mu = 1$) in model A and 2 ($\mu = 2$) in model B. The result shows that both of the magnitude and exceeding behavior are very consistent at P2, P4 and P8. Figure 11.9 shows the EPWP dissipation behavior. We could observe that the dissipation time is slightly different at P2 due to the effect of viscosity of saturation fluid.

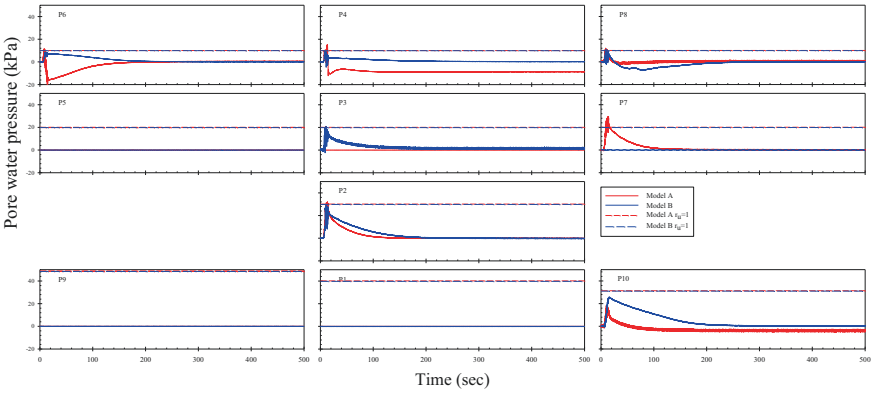

Fig. 11.9 Excess pore water pressure time histories (500 s) of main shaking (s2)

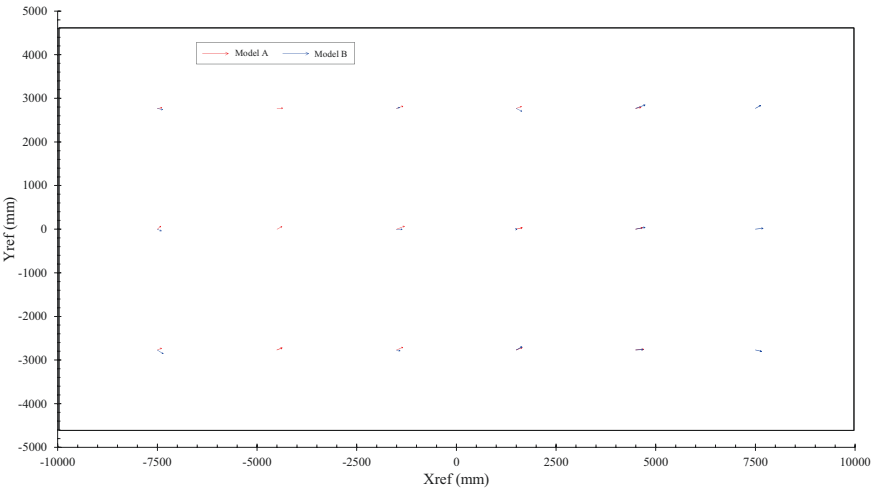

Fig. 11.10 Displacement of surface markers

11.4.3 Surface Displacement

The surface displacement and settlement are expressed in prototype scale by taking scaling factor of 26 ($\mu^{1.5}\eta = 1^{1.5} \times 26$) in model A and 36.77 ($\mu^{1.5}\eta = 2^{1.5} \times 13$) in model B. Figure 11.10 shows the displacement vector of each marker. The maximum displacement happens at middle slope in model A but at downslope in model B. There is lower consistency of surface displacement behavior, both of magnitude and direction, between each model. Figures 11.11 and 11.12 show the settlement of markers. The maximum settlement happens at number 1 marker location (upslope), and maximum upheave induced by accumulation of upslope soil happens at number 6 maker location (downslope) in both models. However, the magnitude and the trend at middle slope are not consistent between each model.

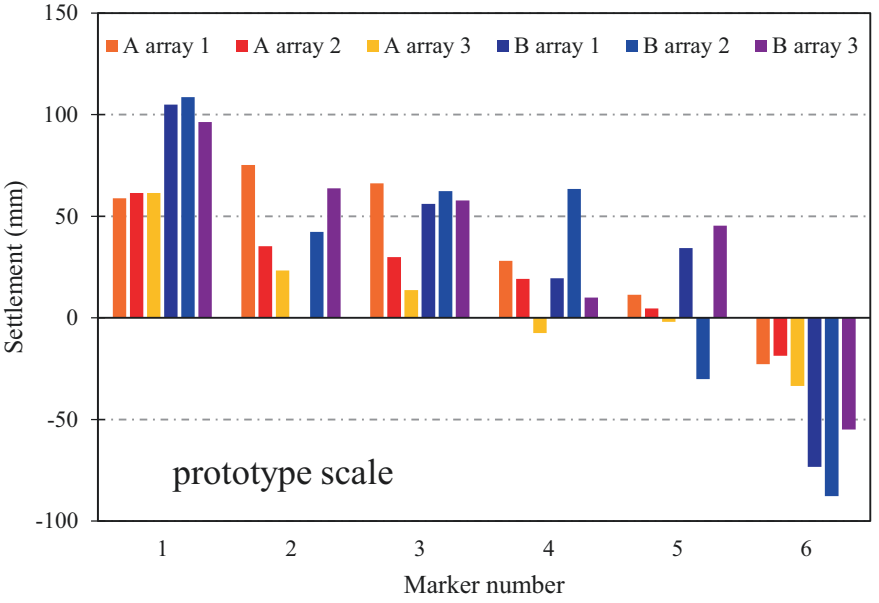

Fig. 11.11 Settlement of all markers

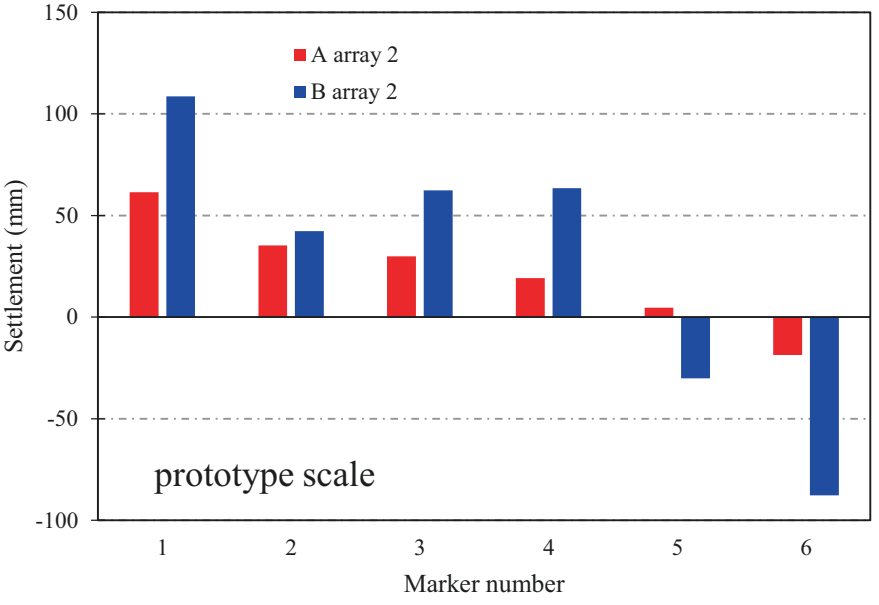

Fig. 11.12 Settlement of array 2 markers

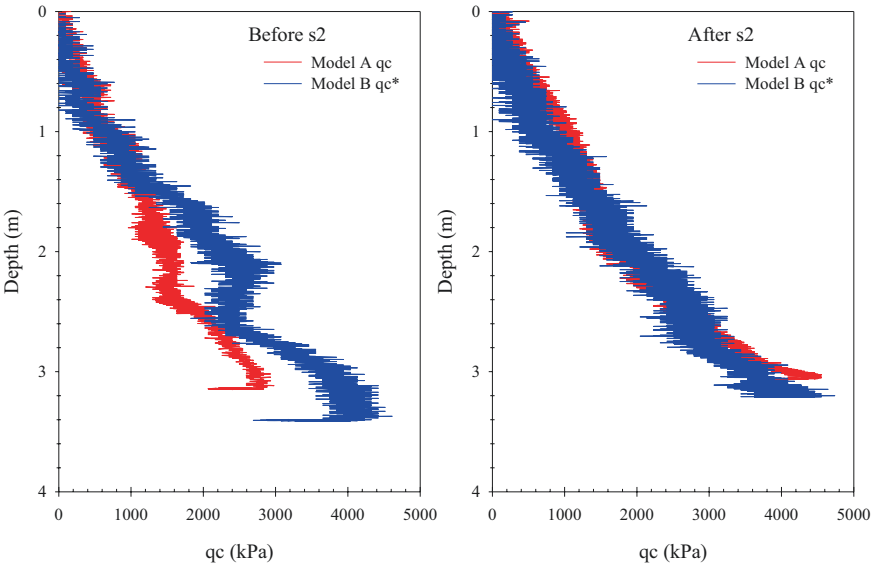

Fig. 11.13 Cone tip resistance (q_c) distribution along the depth

11.4.4 Cone Tip Resistance

The distribution of q_c along the depth is plotted at Fig. 11.13. The q_c is expressed in prototype scale by taking scaling factor of 1 ($\mu = 1$) in model A and 2 ($\mu = 2$) in model B. The value after destructive motion 1 is very consistent between model A and model B. Before destructive motion 1, the value is very consistent at depth 0–1.5 m, but the value is different at depth over 1.5 m. The difference of q_c may be influenced by the speed of penetration. The speed of penetration is not constant because the penetration force applied to CPT is applied by manually adjusting air pressure to cylinder.

11.4.5 Discussion on GSL

In general, the prototype of model B which the 1g virtual scaling factor (μ) is 2 can modeling the prototype of model A. The results of acceleration response, excess pore water pressure behavior, and cone tip resistance between model A and model B are in good agreement with each other. However, the results of acceleration response and surface displacement behavior indicate the consistency of surface soil behavior is low. Therefore, more experiments are needed to validate GSL.

11.4.6 LEAP-UCD-2017 vs. LEAP-ASIA-2019

Figures 11.14 and 11.15 are the acceleration and EPWP time histories of NCU models in LEAP-UCD-2017 (Hung & Liao, 2020). The density of models and the PBA of input motions are different with NCU models in LEAP-ASIA-2019. The density of models is 1651, 1653, and 1653 kg/cm^3 corresponding to NCU 1, NCU 2, and NCU 3 in LEAP-USD-2017. The achieved PBA of motion is 0.265, 0.221, and 0.185g corresponding to NCU 1-m1, NCU 2-m1, and NCU 3-m3. Although density and PBA of models in LEAP-UCD-2017 are denser and larger than models in LEAP-ASIA-2019, the trend of results in both projects is similar.

11.5 Pre-shaking Analysis and Spaghetti Deformation

11.5.1 Shear Velocity

Pre-shaking technique provided by Lee et al. (2012) is used to detect the shear velocity and predominant frequency of soil strata by inputting a non-destructive motion. In both model A and model B, a 3 Hz, PBA = 0.04g, 1 cycle sine wave non-destructive motion was input before and after test. The amplitude and duration of motion are small and short enough so that it would only exceed little or even no excess pore water pressure. Figures 11.16 and 11.17 show the acceleration time histories of both model in s1 and s3.

$$v_s = \frac{L}{\Delta t} \tag{11.1}$$

where v_s = shear velocity (m/s), L = distance (m), Δt = time difference (s).

Shear velocity of soil strata is determined by Formula (11.1). The arrival time of wave is got from each accelerometer time history; afterward, the difference arrival time between each accelerometer can be determined. Moreover, the distance between each accelerometer is given. The shear velocity of soil strata is finally figured out. The results are shown in Fig. 11.18. The average shear velocity is averaged out the shear velocity of 3 arrays. In model A case, the average shear velocity is 367 and 520 m/s before and after destructive motion (s2), respectively. In model B case, the average shear velocity is 296 and 340 m/s before and after destructive motion (s2), respectively. The shear velocity of soil strata is related to the density of soil strata. Denser soil has larger shear velocity, and the density of model A is larger than the density of model B. In addition, the density of soil strata after destructive motion (s2) is supposed to be larger than the density of soil strata before destructive motion (s2). Therefore, the results are reasonable.

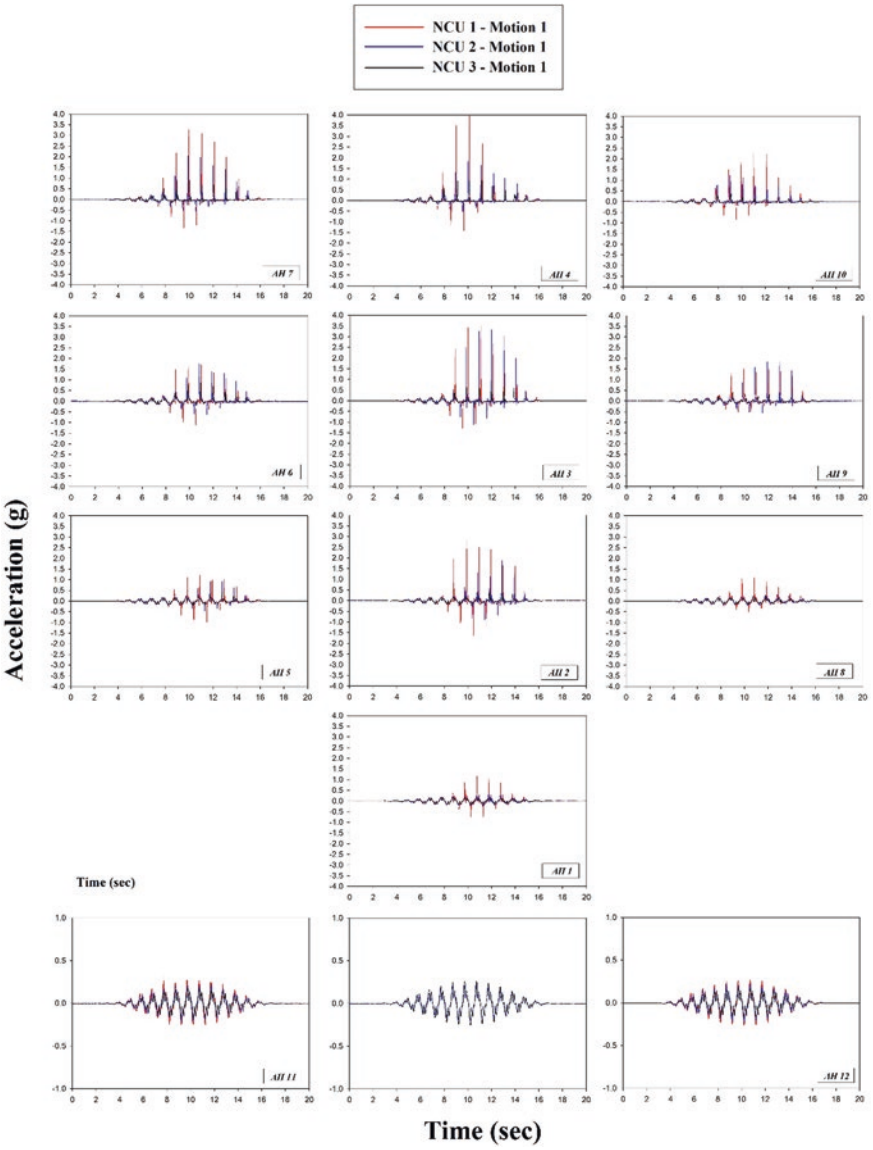

Fig. 11.14 The time histories of acceleration for NCU1-m1, NCU2-m1 and NCU3-m1 in LEAP-UCD-2017

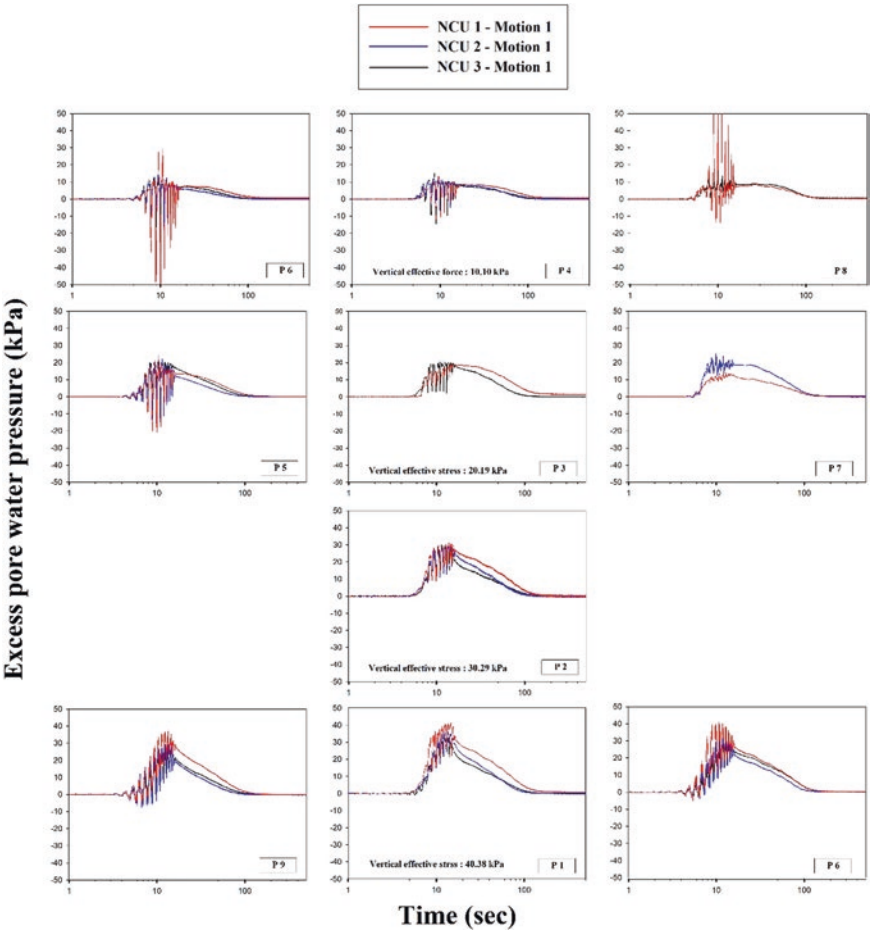

Fig. 11.15 The time histories of pore water pressure for NCU1-m1, NCU2-m1, and NCU3-m1 in LEAP-UCD-2017

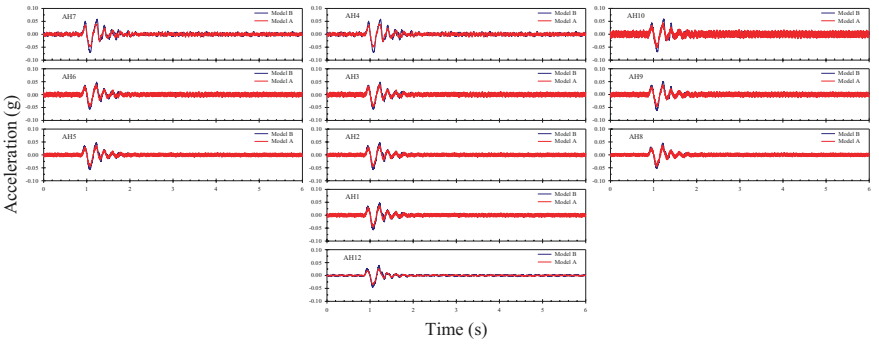

Fig. 11.16 Acceleration time histories of s1 (pre-shaking before main shaking)

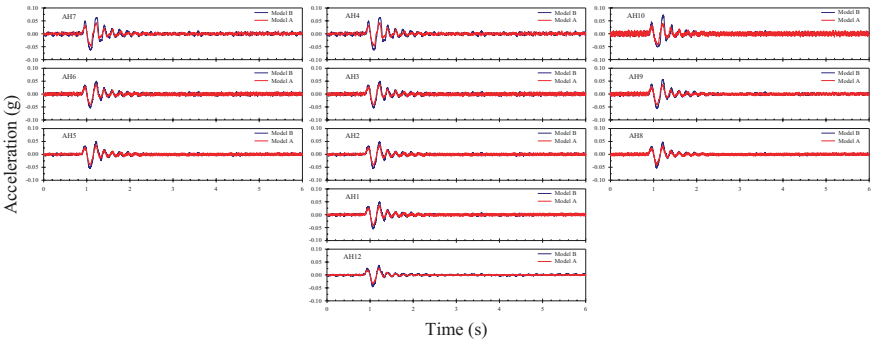

Fig. 11.17 Acceleration time histories of s3 (pre-shaking after main shaking)

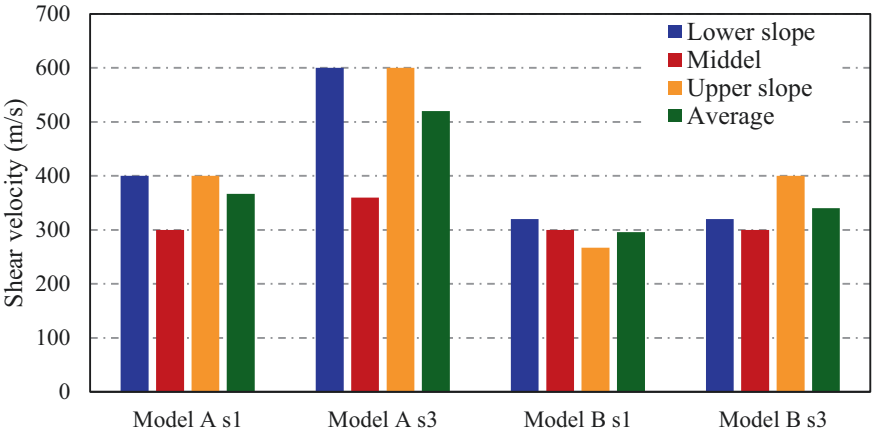

Fig. 11.18 Shear velocity of soil strata before and after main shaking

11.5.2 Predominant Frequency

Transform the free vibration signal of pre-shaking acceleration time histories to frequency domain from time domain via fast Fourier transform. Figure 11.19 shows the Fourier spectra of acceleration time histories in s1 and s3. From Fourier spectra, the predominant frequency of soil strata in model A is 5.25 Hz and in model B is 5.5 Hz. In addition, the frequency of free vibration can be estimated from acceleration time histories. The estimated frequency of free vibration is approximately at the range of 5–6 Hz.

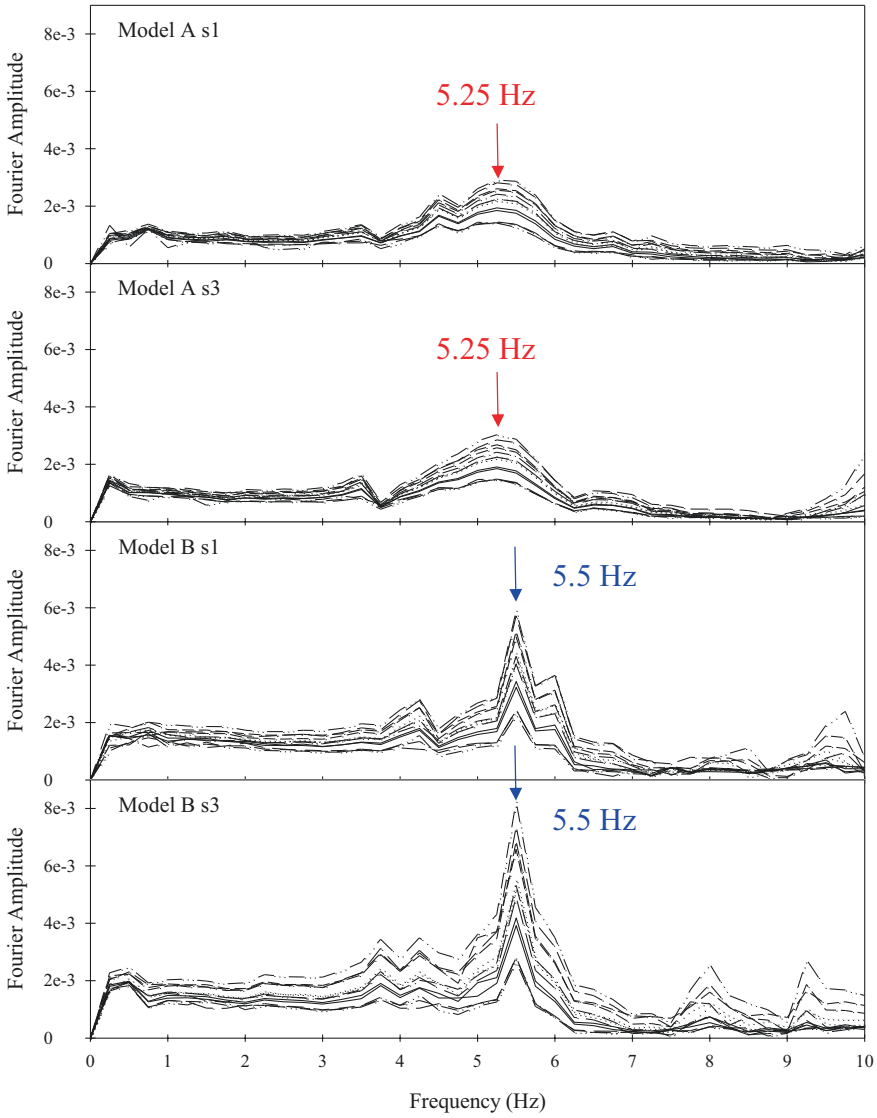

Fig. 11.19 Fourier spectra of acceleration time histories in s1 and s3

11.5.3 Spaghetti Deformation

The spaghettis were penetrated into soil strata during model preparation. The spaghettis were supposed to deform with the soil strata; therefore, the deformation behavior of soil strata can be estimated by the displacement of spaghetti. The soil strata profile is got by cutting model after test. The horizontal displacement of spaghetti along the depth (Fig. 11.20) is determined via image digitalized tool from the

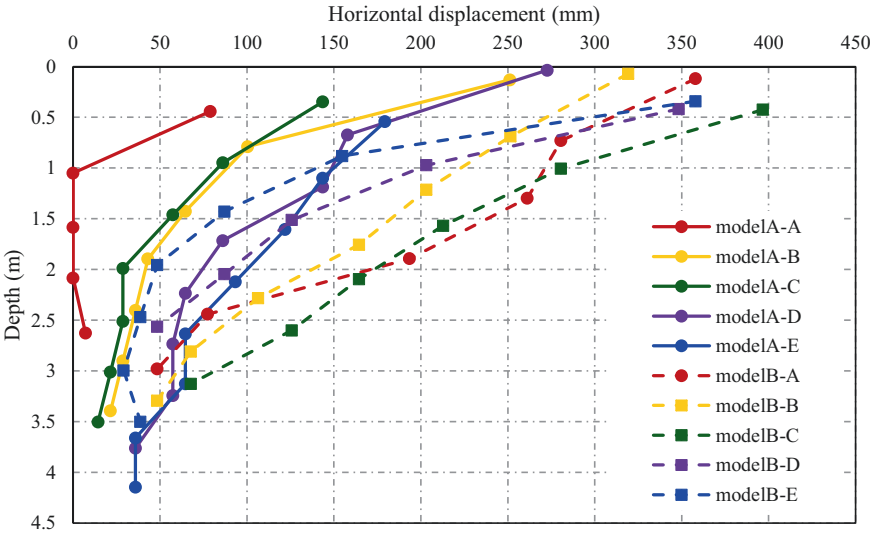

Fig. 11.20 Displacement of spaghetti along the depth after test

soil profile. The result indicates the horizontal displacement of soil decrease with increasing depth in both models, but the displacement in model B is larger than in model A. It shows the generalized scaling factor for displacement may overestimate the among of displacement.

11.6 Conclusions

Two centrifuge modeling tests were conducted to validate the generalized scaling law. Both models are 5°-inclined slope of 4-m-deep-saturated sandy ground model subjected a destructive motion with PBA 0.18 and 0.16g, respectively. Model A adopts centrifuge scaling law with centrifuge scaling factor (η) of 26. Model B adopts generalized scaling law with centrifuge scaling factor (η) of 13 and virtual 1g modeling factor (μ) of 2. The results of acceleration response, excess pore water pressure, and cone tip resistance show the generalized scaling law can simulate the same prototype simulated by centrifuge scaling law well. However, the results of surface displacement and ground displacement show the generalized scaling factor for displacement may overestimate the among of displacement.

Acknowledgement The authors would like to express our gratitude for the financial support from the Ministry of Science and Technology, Taiwan (R.O.C.) (MOST 106-2628-E-008-004 -MY3) and the technical support from the Experimental Center of Civil Engineering, National Central University. These supports made this study and further research possible and efficient.

References

Carey, T. J., Stone, N., & Kutter, B. L. (2020). Grain size analysis and maximum and minimum dry density testing of Ottawa F-65 sand for LEAP-UCD-2017. In *Model tests and numerical simulations of liquefaction and lateral spreading: LEAP-UCD-2017* (pp. 31–44). Springer.

El Ghoraiby, M., Park, H., & Manzari, M. T. (2020). Physical and mechanical properties of Ottawa F65 sand. In *Model tests and numerical simulations of liquefaction and lateral spreading: LEAP-UCD-2017* (pp. 45–67). Springer.

Hung, W. Y., & Liao, T. W. (2020). LEAP-UCD-2017 centrifuge tests at NCU. In *Model tests and numerical simulations of liquefaction and lateral spreading: LEAP-UCD-2017* (pp. 361–384). Springer.

Hung, W.-Y., Huang, J.-X., Lin-Mao, H., & Nguyen, T.-A. (2022). LEAP-UCD-2017 and additional tests at NCU. *Soil Dynamics and Earthquake Engineering, 156*. https://doi.org/10.1016/j.soildyn.2022.107206

Iai, S., Tobita, T., & Nakahara, T. (2005). Generalised scaling relations for dynamic centrifuge tests. *Geotechnique, 55*(5), 355–362.

Kutter, B. L., Carey, T. J., Stone, N., Bonab, M. H., Manzari, M. T., Zeghal, M., Escoffier, S., Haigh, S., Madabhushi, G., Hung, W., Kim, D., Kim, N., Okamura, M., Tobita, T., Ueda, K., & Zhou, Y. G. (2020a). LEAP-UCD-2017 v. 1.01 model specifications. In *Model tests and numerical simulations of liquefaction and lateral spreading: LEAP-UCD-2017* (pp. 3–29). Springer.

Kutter, B. L., Carey, T. J., Stone, N., Zheng, B. L., Gavras, A., Manzari, M. T., Zeghal, M., Abdoun, T., Korre, E., Escoffier, S., Haigh, S., Madabhushi, G., Madabhushi, S., Hung, W., Liao, T., Kim, D. S., Kim, S. N., Ha, J. G., Kim, N. R., Okamura, M., Sjafuddin, A. N., Tobita, T., Ueda, K., Vargas, R., Zhou, Y. G., & Liu, K. (2020b). LEAP-UCD-2017 comparison of centrifuge test results. In *Model tests and numerical simulations of liquefaction and lateral spreading: LEAP-UCD-2017* (pp. 69–103). Springer.

Lee, C. J., Wang, C. R., Wei, Y. C., & Hung, W. Y. (2012). Evolution of the shear wave velocity during shaking modeled in centrifuge shaking table tests. *Bulletin of Earthquake Engineering, 10*, 401–420.